



Article

Easy-to-Fabricate UV-Glue-Based Cascaded Fabry–Perot Fiber Sensor Probe for Temperature Measurement

Xuehao Hu ¹, Hongyu Fu ², Pengcheng Li ², Carlos Marques ³, Chuanxin Teng ⁴, Hang Qu ^{2,*} and Christophe Caucheteur ¹

- ¹ Department of Electromagnetism and Telecommunication, University of Mons, Boulevard Dolez 31, 7000 Mons, Belgium; xuehao.hu@umons.ac.be (X.H.); christophe.caucheteur@umons.ac.be (C.C.)
- ² Research Center for Advanced Optics and Photoelectronics, Department of Physics, College of Science, Shantou University, Shantou 515063, China; 21hyfu@stu.edu.cn (H.F.); pchli@stu.edu.cn (P.L.)
- ³ CICECO—Aveiro Institute of Materials, Physics Department, University of Aveiro, 3810-193 Aveiro, Portugal; carlos.marques@ua.pt
- ⁴ Guangxi Key Laboratory of Optoelectronic Information Processing, Guilin University of Electronic Technology, Guilin 541004, China; cxteng@guet.edu.cn
- * Correspondence: haqux@stu.edu.cn

Abstract: In this paper, we propose an in-line fiber sensor probe based on UV-glue-assisted cascaded Fabry–Perot cavities for temperature measurement. The UV-curable adhesive in the sensing cavity plays an important role due to its high thermo-optic coefficient. We show that the temperature sensitivity depends on the optical path length difference between both cavities. We report a maximum value of 12.57 nm/°C in the range of 20 to 30 °C. This original sensor architecture features a low cost and simple structure that can be straightforwardly manufactured with readily available materials and a short production time.

Keywords: F-P cavity; UV-curable adhesive; temperature sensor



Citation: Hu, X.; Fu, H.; Li, P.; Marques, C.; Teng, C.; Qu, H.; Caucheteur, C. Easy-to-Fabricate UV-Glue-Based Cascaded Fabry–Perot Fiber Sensor Probe for Temperature Measurement. *Photonics* **2024**, *11*, 111. <https://doi.org/10.3390/photonics11020111>

Received: 7 December 2023

Revised: 18 January 2024

Accepted: 23 January 2024

Published: 25 January 2024



Copyright: © 2024 by the authors. Licensee MDPI, Basel, Switzerland. This article is an open access article distributed under the terms and conditions of the Creative Commons Attribution (CC BY) license (<https://creativecommons.org/licenses/by/4.0/>).

1. Introduction

Optical fiber sensors have been demonstrated to outperform conventional technologies in various applications, including physical, biochemical, medical/pharmaceutical, and environmental fields, among others [1]. These sensors have been extensively utilized to detect a variety of parameters, such as humidity, strain, refractive index, and temperature, to name a few [2,3]. Numerous applications have been conducted to demonstrate their efficacy and usefulness in these industries. To date, for the measurement of temperature, different fiber sensing mechanisms have been involved, such as intensity modulation sensor, Fabry–Perot (F-P) interferometric sensors, Mach–Zehnder interferometric sensors, and grating-based sensors (fiber Bragg grating, long period grating, and tilted fiber grating) [4–6]. Among these sensing scenarios, the F-P interferometric sensors play an important role due to the ease of fabrication and relatively high sensitivities.

Recently, a high-temperature F-P interferometric sensor under Co-60 γ irradiation was proposed by Lyu et al. This sensor was composed of an angled silica multi-mode fiber (MMF), a thin sapphire wafer, and a silica casing. Temperature measurements up to 800 °C were presented with a sensitivity of 29.9 pm/°C [7]. Domínguez-Flores presented an in-fiber F-P interferometer fabricated by splicing a microsegment of capillary fiber between two single-mode fibers (SMFs) and then embedding the structure in a mold made of polyester resin. The sensor sensitivity was up to 327.3 pm/°C in the temperature range of 20 °C to 35 °C [8]. He et al. fabricated an F-P interferometric sensor by encapsulating a microfiber and an SMF in a silica capillary with curable polydimethylsiloxane (PDMS). A higher temperature sensitivity of 6.386 nm/°C in the range from 42 °C to 54 °C was obtained [9]. Zhang et al. proposed a temperature sensor that fills UV glue in a capillary

to form an F-P cavity. Although this sensor has the advantage of a simple structure, its sensitivity is limited to $-1.014 \text{ nm}/^\circ\text{C}$ [10]. It is obvious that the resin plays an important role in increasing the temperature sensitivity due to the high thermal-optic coefficient.

Compared to traditional interferometric sensors, the Vernier effect applied to fiber interferometers has drawn increasing attention from researchers [11,12]. This effect stems from the spectral overlap of two cascaded interferometers with slightly detuned free spectral ranges (FSRs) or interference frequencies [13]. Generally, one of the interferometers works as a reference unit, while the other one acts as a sensing unit [14]. The output signal of the configuration with the Vernier effect is the overlap of the two interferometric spectra with periodic envelopes (or the so-called “beats”). The temperature perturbations applied to the sensing element could induce dramatic shifts of the envelopes, considerably amplifying the sensitivity as compared to the sensors based on a single interferometric structure.

Gomes et al. developed a miniaturized Vernier-effect optical fiber F-P interferometer temperature sensor with a sensitivity of $-654 \text{ pm}/^\circ\text{C}$ that is 60 folds higher than that of a normal F-P interferometer. The Vernier effect was triggered due to the presence of multiple modes in the F-P cavity. However, this cavity was intricately fabricated by focused ion beam milling of the end of a tapered MMF, thus generating multiple F-P interferometers with shifted frequencies [15]. Zhang et al. demonstrated an ultrasensitive fiber temperature sensor with a sensitivity of $\sim 67.35 \text{ nm}/^\circ\text{C}$ based on two cascaded cavities with slight length differences. The sensing cavity was composed of a cleaved fiber end-face and thermally expandable UV-cured adhesive mounted inside a ceramic ferrule for the length change of the sensing cavity [16]. This work shows the added value of the UV-cured adhesive. However, the length of the sensing cavity was difficult to control inside the ferrule and the fabrication process of the sensing cavity was relatively complicated. Similarly, Huang et al. presented an enhanced Vernier effect with a sensitivity of $-13.09 \text{ nm}/^\circ\text{C}$ based on two parallel F-P interferometers with opposite temperature sensitivity. Since AB glue and polyimide solution had to be filled in the capillary, the sensor fabrication process is rather sophisticated [17].

In this paper, we propose two in-line fiber sensor probes based on cascaded F-P cavities for measurement of temperature. The UV-curable adhesive in the sensing cavity plays an important role due to the high thermo-optic coefficient. The two sensors with different cavity lengths show different performances. For sample 1, a temperature sensitivity of $4.54 \text{ nm}/^\circ\text{C}$ is obtained in the range of 20 to 40 $^\circ\text{C}$. For sample 2, due to a smaller optical path length difference between two cavities, a much higher sensitivity of $12.57 \text{ nm}/^\circ\text{C}$ is achieved in the range of 20 to 30 $^\circ\text{C}$. This proposed sensor features a simple structure, low cost, straightforward manufacturing process, readily available materials, and shorter production time, which can be applied for temperature measurement in specialized fields, such as biochemical engineering, medical care, and nuclear testing.

2. The Principle of a Cascaded Fabry–Perot Sensor

The working principle of this proposed fiber sensor is first based on an F-P interferometer fiber sensor with a single cavity, whose FSR is expressed [18,19] by:

$$\text{FSR} = \frac{\lambda^2}{2nL} \quad (1)$$

where λ , n , and L represent the light wavelength in vacuum, the refractive index inside the cavity, and the cavity length, respectively. Then, a second cavity is relayed on to generate Vernier effect, thus forming spectral envelopes. The FSR of the envelop can be written as follows [20,21]:

$$\text{FSR}_e = \frac{\text{FSR}_1 \times \text{FSR}_2}{|\text{FSR}_1 - \text{FSR}_2|} \quad (2)$$

The sensitivity amplification factor is thus expressed as follows [16]:

$$M = \frac{FSR_e}{FSR_1} = \frac{FSR_2}{|FSR_1 - FSR_2|} = \frac{n_1 L_1}{|n_1 L_1 - n_2 L_2|} \quad (3)$$

where FSR_1 and FSR_2 represent the FSR for interference spectra of $Cavity_1$ and $Cavity_2$, and FSR_e represents the FSR of the spectral envelope in the transmission spectrum. Notably, if two cavities have similar optical lengths (OLs), the sensitivity of the cascaded F-P fiber sensor can be dramatically enhanced and the FSR_e of the envelop is large.

3. Manufacturing of the Sensor

The structure of the proposed sensor is illustrated in Figure 1. An SMF pigtail (SMF_1) and a small segment of SMF (SMF_2) are assembled by UV glue while SMF_2 is fusion-spliced with a segment of capillary fiber. The UV glue between SMF_1 and SMF_2 forms the resonant $Cavity_1$ with a length of L_1 . SMF_2 forms the resonant $Cavity_2$ with a length L_2 and $Cavity_1$ and $Cavity_2$ together form combined $Cavity_3$. The interface between the SMF_1 and the UV glue constitutes $Mirror_1$ and the interface between the UV glue and SMF_2 constitutes $Mirror_2$. The interface between SMF_2 and the air inside the capillary forms $Mirror_3$. In this case, three F-P cavities are obtained. $Cavity_1$ is composed of the UV glue whose optical length is very sensitive to temperature. $Cavity_2$ is composed of the SMF_2 . Thus, $Cavity_3$ is a combination of $Cavity_1$ and $Cavity_2$ with a cavity length of $L_1 + L_2$. The schematic of the sensor probe is depicted in Figure 1.

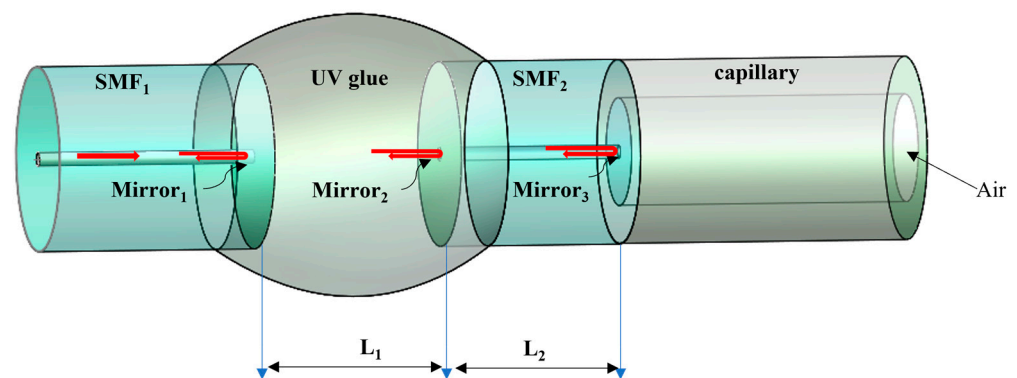


Figure 1. Schematic of the Vernier-based cascaded F-P cavity fiber sensor for measurement of temperature.

4. Temperature Measurements

4.1. Experimental Setup

The sensor probe used in this work was fabricated as the following steps. Firstly, a SMF was spliced with a silica capillary fiber (Polymicro Technologies, Phoenix, AZ, USA, TSP075150, inner diameter: 75 μm , outer diameter: 124 μm) using a fusion splicer (Fujikura, Duncan, SC, USA, FSM-100P). During the discharge process, the electric arc was not positioned at the interface between the capillary and the SMF, but mostly on the SMF side by using the manual mode of the fusion splicer to avoid the collapse of the capillary. Then, the SMF was cleaved into a designated length using a fiber cleaver with the aid of a long working-distance microscope. The cleaved SMF and another SMF pigtail were then mounted on the three-axis micro-positioning stage (Thorlabs, Newton, NJ, USA, MBT616D) that is used to align these two fiber pieces with a gap of proper length between them by the optical microscope as well. Afterward, UV-curable adhesive (Norland, Jamesburg, NJ, USA, NOA 73) was filled in the gap between the two SMFs and the gap was further finely adjusted to obtain an appropriate spectrum envelope by monitoring the reflected spectrum. Finally, The UV-curable adhesive was cured for ~ 30 s using a UV lamp (SJMAEA, Shanghai, China, wavelength: 365 nm) with an illumination intensity of 12 mW/cm^2 . The optical microscopic images of the two samples are shown in the insets of Figure 2.

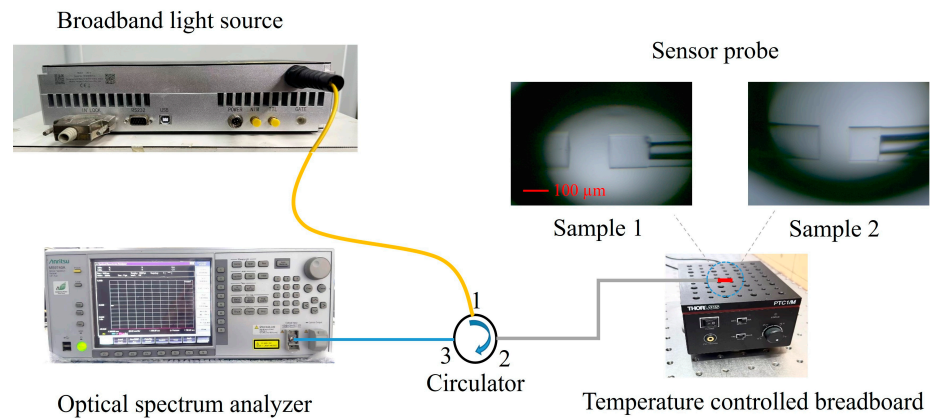


Figure 2. Schematic of the interrogation set-up for temperature measurements. The insets are the microscopic images of the sensor probes.

To characterize the sensor performance, the sensor probes were immobilized on the temperature-controlling breadboard (Thorlabs, PTC1/M) with a readout resolution of ± 0.001 °C. To minimize the response time, the sensor probes were immersed in UV glue without curing between two coverslips to reduce the influence of air humidity. A reflected spectral interrogation system, which included a broadband light source (BBS) (YSL Photonics, Wuhan, China, SC-5-FC), a circulator, and an optical spectrum analyzer (OSA) (Anritsu, Kanagawa, Japan, MS9740A), was used to monitor the evolutions of reflection spectra in response to temperature variations, as shown in Figure 2. The location of the envelope is determined by the wavelength of the peak or the valley in the envelope via Lorentz fitting.

4.2. The Measurement Results for Sample 1

For sample 1, the L_1 and L_2 were set to ~ 142 μm and ~ 162 μm , respectively, and a series of reflection spectra with FSR of ~ 50 nm were recorded at a step of 1 °C in the temperature range of 20–40 °C, as shown in Figure 3. It is obvious that the envelope has an extremely obvious red shift. The red arrows in Figure 3a indicate the shifts of the envelope. This experiment was repeated for another two times, showing good repeatability. The average sensitivity of 4.54 ± 0.13 nm/°C was obtained by lineal fitting.

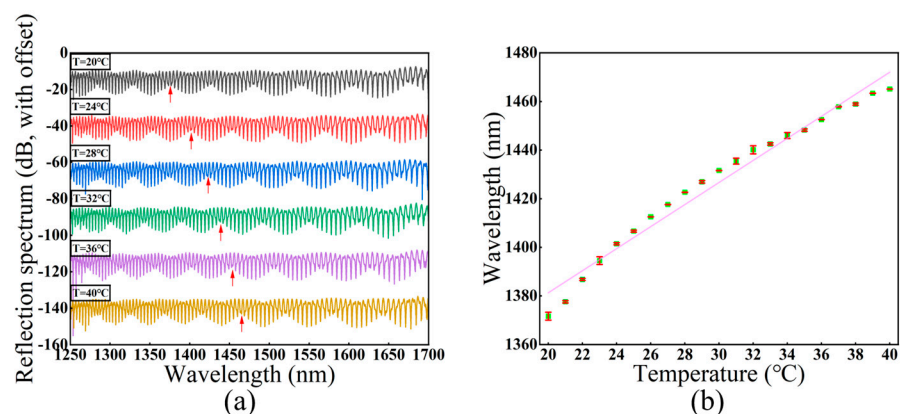


Figure 3. (a) Experimental spectral evolution of sample 1 (with offset) and (b) linear fit of the envelope as a function of temperature from 20 to 40 °C.

With the structural parameters above, the theoretical calculation of the reflected spectra evolution as a function of different temperatures can be conducted using the methodology reported in Ref. [21]. The thermal expansion coefficients (TECs) of the UV glue and SMF were 2.2×10^{-4} and 4.1×10^{-7} [22], respectively. The thermal-optic coefficients (TOCs)

of the UV glue and SMF were set to be -7.0×10^{-4} and 7.97×10^{-6} [22], respectively. The initial refractive indices of the UV glue and SMF at 25 °C were set at 1.54 and 1.448, respectively. As SMF₂ in Cavity₂ is coated by cured UV glue (see Figure 2), the TEC of the mixture can be calculated by [23]:

$$\alpha_{\text{Mix}} = \frac{\alpha_{\text{Silica}} + \alpha_{\text{Glue}} E_{\text{Glue}} / E_{\text{Silica}}}{1 + E_{\text{Glue}} / E_{\text{Silica}}} \quad (4)$$

where α_{Silica} and α_{Glue} represent the TEC of the silica fiber and UV glue, respectively. E_{Silica} and E_{Glue} represent the Young’s modulus of the silica fiber and UV glue, respectively. Thus, α_{Mix} is the TEC of the mixed material. However, since the Young’s modulus of the silica fiber is 69.2 Gpa [24], which is much greater than 0.01 Gpa for the UV glue, the TEC of the mixture is proximately equal to that of the silica fiber and thus the influence from the UV glue is ignored. Considering these aforementioned parameters, the simulation results are shown in Figure 4, showing a similar FSR and sensitivity of ~ 54 nm and 4.96 ± 0.04 nm/°C, respectively, which are similar to the experimental ones. The red arrows in Figure 4a indicate the shifts of the envelope.

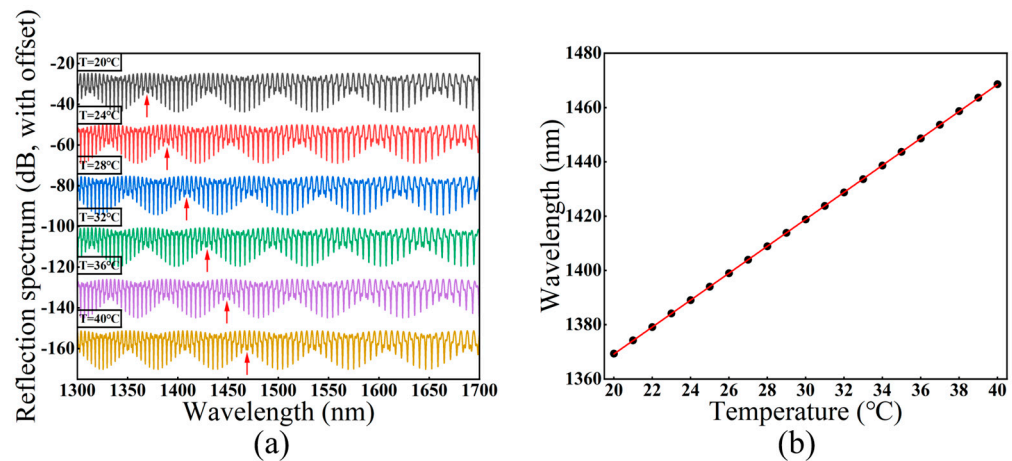


Figure 4. (a) Simulated spectral evolution of sample 1 (with offset) and (b) lineal fit of the envelope as a function of temperature from 20 to 40 °C.

4.3. The Measurement Results for Sample 2

For sample 2, the values of L_1 and L_2 were set to ~ 118 μm and ~ 129 μm , respectively. A series of reflected spectra with an FSR of ~ 156 nm were recorded within a temperature range of 20 to 30 °C, with a step of 1 °C, as illustrated in Figure 5. The red arrows in Figure 5a indicate the shifts of the envelope. As with sample 1, this experiment was conducted for three times in total, with good repeatability. With the lineal fitting, an average sensitivity of 12.57 ± 0.52 nm/°C was obtained. It is worth mentioning that the sensing range could be extended as long as the envelop peak we monitored is within the spectral range of the OSA.

Based on the parameters mentioned above, simulation results are presented in Figure 6, indicating a comparable FSR and sensitivity of ~ 167 nm and 12.51 ± 0.03 nm/°C, respectively. The red arrows in Figure 6a indicate the shifts of the envelope. The OL variations of both cavities are listed in Table 1, showing a much higher absolute variation of ~ -426.3 nm for Cavity₁ than ~ 11 nm For Cavity₂. Thus, compared to the TEC, the TOC of the UV glue plays a more important role for this temperature sensing.

By comparing both samples, it is found that the temperature sensitivity of Sample 2 is three times higher than that of Sample 1. This is mainly due to the smaller OL difference between Cavity₁ and Cavity₂ (~ 18 μm for sample 1 and ~ 5 μm for sample 2) with an enhanced amplification factor, according to Equations (1)–(3). Moreover, the sensitivity can be further improved by reducing the difference in OL between the two cascaded cavities. Theoretically, this sensitivity can actually become infinite. However, this is also the

result of a significant increase in the envelope FSR, which may extend beyond the spectral measurement range. Thus, a trade-off has to be made between higher sensitivity and a larger sensing range.

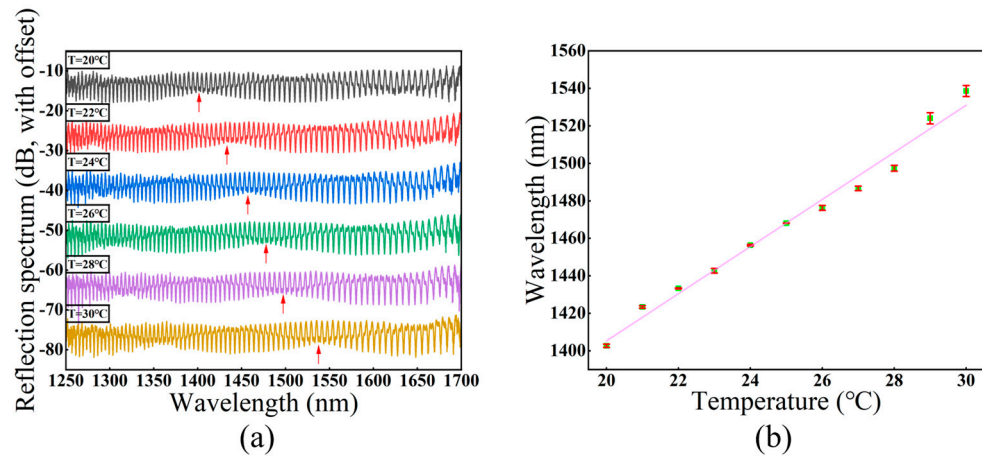


Figure 5. (a) Experimental spectral evolution of sample 2 (with offset) and (b) linear fit of the envelope as a function of temperature from 20 to 30 °C.

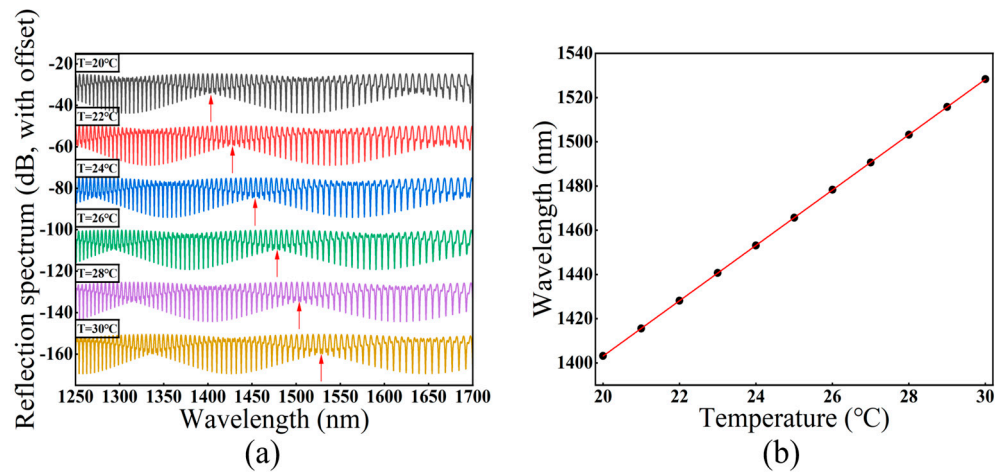


Figure 6. (a) Simulated spectral evolution of sample 2 (with offset) and (b) lineal fit of the envelope as a function of temperature from 20 to 30 °C.

Table 1. Optical length variations for Sample 2 as a function of temperature from 20 to 30 °C.

Temperature (°C)	20	22	24	26	28	30
OL change of Cavity ₁ (nm)	0	−85.0	−170.2	−255.4	−340.8	−426.3
OL change of Cavity ₂ (nm)	0	2.2	4.4	6.6	8.8	11

We also carried out Fast Fourier Transform calculations on the experimental spectra of the two samples measured at 24 °C (Figure 7a,b). The Vernier effect could be virtually considered as the superposition of interference spectra of the individual resonant F-P cavities in the sensor probe. Therefore, this FFT spectrum could reflect information with respect to the FSRs of the interference spectra of the individual F-P cavities. For Sample 1 (Figure 7a), the peak 1 centered at $\sim 0.195 \text{ nm}^{-1}$ in the spatial frequency domain corresponds to the FSR of the interference spectra of Cavity₁ and Cavity₂, which is $\sim 5.15 \text{ nm}$ at 1500 nm. The peak 2 centered at $\sim 0.35 \text{ nm}^{-1}$ corresponds to the FSR of the spectrum of Cavity₃, which is $\sim 2.99 \text{ nm}$ at 1500 nm calculated from Equation (1). These two peaks are relatively wide since the FSR is dependent on wavelength in the wide spectral range (1250–1700 nm).

For sample 2 (Figure 7b), the peak 1 and peak 2 centered at $\sim 0.166 \text{ nm}^{-1}$ and $\sim 0.330 \text{ nm}^{-1}$, which corresponds to the Cavity₁ FSR ($\sim 6.19 \text{ nm}$ at 1500 nm) and Cavity₃ FSR ($\sim 3.05 \text{ nm}$ at 1500 nm), respectively.

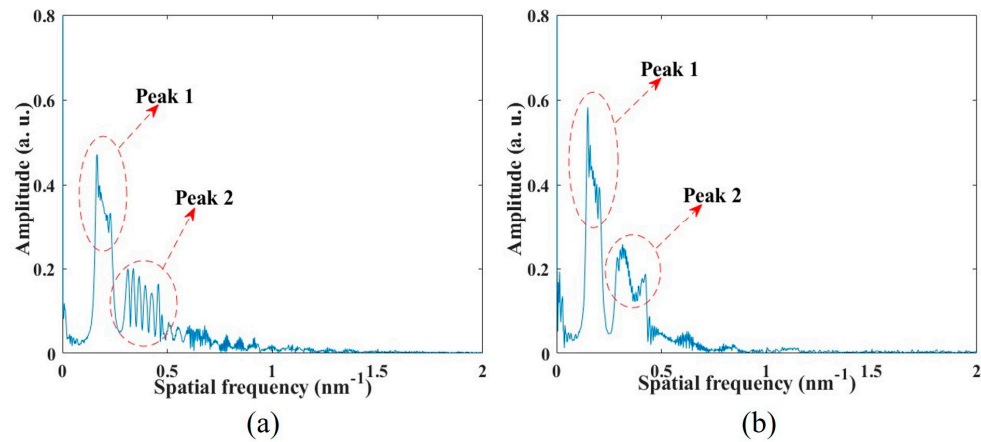


Figure 7. Spatial frequency spectra were obtained by applying FFT to the transmission spectrum of Sample 1 (a) and Sample 2 (b) measured at $24 \text{ }^\circ\text{C}$.

5. Discussion

The capillary fiber actually acts as a supporting structure when gluing the SMF segment with lead-in SMF. There are two reasons for the selection of this silica capillary: (1) the inner radius of $75 \text{ }\mu\text{m}$ is much larger than $\sim 8 \text{ }\mu\text{m}$ for a single mode fiber core, which facilitates the visual identification of SMF-capillary fiber interface during the fiber fusion process before fiber cutting, and (2) the outer radius of $124 \text{ }\mu\text{m}$ virtually matches that of the SMF ($125 \text{ }\mu\text{m}$) for a single mode fiber cladding inducing a good splice.

The main purpose of the current paper is to show how to use the popular SMF and UV glue on the market to amplify the sensitivity through the Vernier effect. Furthermore, the whole sensor probe is encapsulated by the UV glue, so that the strength is improved. It is also worth mentioning that during the fabrication process of the sensor probes, the length of Cavity₂ can be more precisely optimized by monitoring the reflected spectra as another reference in addition to the monitoring of the translation stage displacement by the optical microscope. The fact that the refractive index of the adhesive in the liquid phase is 0.02 lower than the counterpart in the solid phase after curing has to be considered. In terms of the temperature sensing range, as the bonds of the UV glue will initially withstand $-15 \text{ }^\circ\text{C}$ to $60 \text{ }^\circ\text{C}$ and $-60 \text{ }^\circ\text{C}$ to $90 \text{ }^\circ\text{C}$ after aging [25], we assume the operation range of this sensor probe could be extended from $-60 \text{ }^\circ\text{C}$ to $90 \text{ }^\circ\text{C}$. Compared to various temperature sensors previously reported, this proposed sensor is structurally simpler with real-time monitored spectra during the fabrication process thanks to the curable UV adhesive. The sensor with cascaded F-P cavities is compared in Table 2.

Table 2. Performance comparison of temperature sensors with cascaded F-P cavities.

Sensitivity (nm/ $^\circ\text{C}$)	Temperature Range ($^\circ\text{C}$)	Cavity Structure	Fabrication Difficulty	Reference
6.386	42–54	PDMS-MF	medium	[9]
−13.09	40–58	Glue-capillary	high	[17]
16.51	27–41	PDMS-SMF	Medium	[26]
−9.9	50–52	HB fiber-SMF	medium	[27]
54.4×10^{-3}	40–80	Adhesive-HCF	medium	[28]
−14.6	50–60	PDMS-SMF	medium	[29]
-183.99×10^{-3}	38–100	Tube-SMF	low	[30]
19.55	23–31	LC-SMF	high	[31]

Table 2. Cont.

Sensitivity (nm/°C)	Temperature Range (°C)	Cavity Structure	Fabrication Difficulty	Reference
1.808	30–45	PDMS-HCF	medium	[32]
17.758	40–70	PDMS-HCF	medium	[33]
11.93	40–46	SMF-double-groove cavity with PDMS	Middle	[34]
7.61	34–39	SMF-tube with PDMS	Middle	[35]
4.54	20–40	Glue-SMF	low	This work
12.57	20–30	Glue-SMF	low	This work

High birefringence (HB); Microfiber (MF); Hollow core fiber (HCF); Liquid crystal (LC).

6. Conclusions

In summary, we developed a highly sensitive temperature sensor based on the F-P cavity and the Vernier effect, achieving a sensitivity of 12.57 nm/°C. It has been proved that the UV-curable adhesive in the sensing cavity plays an important role due to the high thermo-optic coefficient. Our method is more convenient and cost-effective than previous sensors, as it only requires ordinary SMFs and capillaries and uses readily available NOA 73 glue with a short curing time. Moreover, we can control the cavity length precisely by both optical microscopes and optical spectra during the splice process, making it easier to optimize the different of the two cavities.

Author Contributions: Conceptualization, H.Q. and X.H.; methodology, X.H. and H.F.; validation, X.H. and H.F.; investigation, H.F. and H.Q.; writing—original draft preparation, H.F. and X.H.; writing—review and editing, H.Q., C.M., C.T. and C.C.; supervision, P.L., H.Q. and X.H.; funding acquisition, P.L., X.H., H.Q., C.T., C.M. and C.C. All authors have read and agreed to the published version of the manuscript.

Funding: The Fonds de la Recherche Scientifique (F.R.S.-FNRS) under the Postdoctoral Researcher grant (Chargé de Recherches) of Xuehao Hu and the Senior Research Associate Position of Christophe Caucheteur; Natural Science Foundation of Guangxi Province (2023GXNSFDA026040); Science and Technology Department of Guangdong Province (2022A1515012571); National Natural Science Foundation of China (12074239); and Shantou University (NTF22026, NTF23011). This work was also supported within the scope of the projects CICECO-Aveiro Institute of Materials, UIDB/50011/2020 (DOI 10.54499/UIDB/50011/2020), UIDP/50011/2020 (DOI 10.54499/UIDP/50011/2020) & LA/P/0006/2020 (DOI 10.54499/LA/P/0006/2020), financed by national funds through the FCT/MCTES (PID-DAC); DigiAqua (PTDC/EEI-EEE/0415/2021).

Institutional Review Board Statement: Not applicable.

Informed Consent Statement: Not applicable.

Data Availability Statement: Data underlying the results presented in this paper are not publicly available at this time but may be obtained from the authors upon reasonable request.

Conflicts of Interest: The authors declare no conflicts of interest.

References

1. Ferreira, M.S.; Coelho, L.; Schuster, K.; Kobelke, J.; Santos, J.L.; Frazão, O. Fabry-Perot cavity based on a diaphragm-free hollow-core silica tube. *Opt. Lett.* **2011**, *36*, 4029. [[CrossRef](#)] [[PubMed](#)]
2. Sun, B.; Wang, Y.; Qu, J.; Liao, C.; Yin, G.; He, J.; Zhou, J.; Tang, J.; Liu, S.; Li, Z. Simultaneous measurement of pressure and temperature by employing Fabry-Perot interferometer based on pendant polymer droplet. *Opt. Express* **2015**, *23*, 1906. [[CrossRef](#)] [[PubMed](#)]
3. Shivananju, B.N.; Yamdagni, S.; Fazuldeen, R.; Kumar, A.K.S.; Nithin, S.P.; Varma, M.M.; Asokan, S. Highly Sensitive Carbon Nanotubes Coated Etched Fiber Bragg Grating Sensor for Humidity Sensing. *IEEE Sens. J.* **2014**, *14*, 2615. [[CrossRef](#)]
4. Islam, M.R.; Ali, M.M.; Lai, M.-H.; Lim, K.-S.; Ahmad, H. Chronology of Fabry-Perot interferometer fiber-optic sensors and their applications: A review. *Sensors* **2014**, *14*, 7451. [[CrossRef](#)] [[PubMed](#)]

5. Niu, H.; Zhang, S.; Chen, W.; Liu, Y.; Li, X.; Yan, Y.; Wang, S.; Geng, T.; Sun, W.; Yuan, L. Optical fiber sensors based on core-offset structure: A review. *IEEE Sens. J.* **2021**, *21*, 22388. [[CrossRef](#)]
6. Grattan, K.T.V.; Sun, T. Fiber optic sensor technology: An overview. *Sens. Actuator A Phys.* **2000**, *82*, 40. [[CrossRef](#)]
7. Lyu, D.; Peng, J.; Huang, Q.; Zheng, W.; Xiong, L.; Yang, M. Radiation-Resistant Optical Fiber Fabry-Perot Interferometer Used for High-Temperature Sensing. *IEEE Sens. J.* **2021**, *21*, 57. [[CrossRef](#)]
8. Domínguez-Flores, C.E.; Monzón-Hernández, D.; Moreno-Basulto, J.I.; Rodríguez-Quiroz, O.; Minkovich, V.P.; López-Cortés, D.; Hernández-Romano, I. Real-Time Temperature Sensor Based on In-Fiber Fabry-Perot Interferometer Embedded in a Resin. *J. Light. Technol.* **2019**, *37*, 1084. [[CrossRef](#)]
9. Li, J.; Li, Z.; Yang, J.; Zhang, Y.; Ren, C. Microfiber Fabry-Perot interferometer used as a temperature sensor and an optical modulator. *Opt. Laser Technol.* **2020**, *129*, 106296. [[CrossRef](#)]
10. Zhang, C.; Cui, G.; Miao, C.; Zhang, S.; Li, H.; Zhao, J.; Wu, J. A Fabry-Perot temperature sensor sealed with thermo-sensitive polymer. *Results Opt.* **2021**, *5*, 100163. [[CrossRef](#)]
11. Zhang, P.; Tang, M.; Gao, F.; Zhu, B.; Zhao, Z.; Duan, L.; Fu, S.; Ouyang, J.; Wei, H.; Shum, P.P.; et al. Simplified hollow-core fiber-based Fabry-Perot interferometer with modified Vernier effect for highly sensitive high-temperature measurement. *IEEE Photonics J.* **2015**, *7*, 7100210. [[CrossRef](#)]
12. Chen, Y.; Zhao, L.; Hao, S.; Tang, J. Advanced fiber sensors based on the vernier effect. *Sensors* **2022**, *22*, 2694. [[CrossRef](#)] [[PubMed](#)]
13. Gomes, A.D.; Bartelt, H.; Frazão, O. Optical Vernier effect: Recent advances and developments. *Laser Photonics Rev.* **2021**, *15*, 2000588. [[CrossRef](#)]
14. Dai, M.; Chen, Z.; Zhao, Y.; Mu, X.; Liu, X.; Gandhi, M.S.A.; Li, Q.; Lu, S.; Liu, S.; Fu, H.Y. Fiber optic temperature sensor with online controllable sensitivity based on Vernier effect. *IEEE Sens. J.* **2021**, *21*, 21555. [[CrossRef](#)]
15. Gomes, A.D.; Becker, M.; Dellith, J.; Zibaii, M.I.; Latifi, H.; Rothhardt, M.; Bartelt, H.; Frazão, O. Multimode Fabry-Perot Interferometer Probe Based on Vernier Effect for Enhanced Temperature Sensing. *Sensors* **2019**, *19*, 453. [[CrossRef](#)] [[PubMed](#)]
16. Zhang, J.; Liao, H.; Lu, P.; Jiang, X.; Fu, X.; Ni, W.; Liu, D.; Zhang, J. Ultrasensitive Temperature Sensor With Cascaded Fiber Optic Fabry-Perot Interferometers Based on Vernier Effect. *IEEE Photonics J.* **2018**, *10*, 6803411. [[CrossRef](#)]
17. Huang, H.; Zhu, X.; Jiang, C.; Chen, H.; Song, J.; Wang, Y.; Sun, S. High sensitivity temperature sensor based on enhanced Vernier effect through two parallel Fabry-Perot cavities. *Appl. Opt.* **2023**, *62*, 275. [[CrossRef](#)] [[PubMed](#)]
18. Gomes, A.D.; Ferreira, M.S.; Bierlich, J.; Kobelke, J.; Rothhardt, M.; Bartelt, H.; Frazão, O. Optical Harmonic Vernier Effect: A New Tool for High Performance Interferometric Fibre Sensors. *Sensors* **2019**, *19*, 5431. [[CrossRef](#)]
19. Li, Y.; Zhao, C.; Xu, B.; Wang, D.; Yang, M. Optical cascaded Fabry-Perot interferometer hydrogen sensor based on vernier effect. *Opt. Commun.* **2018**, *414*, 166. [[CrossRef](#)]
20. Salceda-Delgado, G.; Van Newkirk, A.; Antonio-Lopez, J.E.; Martinez-Rios, A.; Schülzgen, A.; Amezcua-Correa, R. Optical Capillary Fiber Mode Interferometer for Pressure Sensing. *IEEE Sens. J.* **2020**, *20*, 2253. [[CrossRef](#)]
21. Qiu, H.; Jiang, J.; Yao, L.; Dai, Z.; Liu, Z.; Qu, H.; Hu, X. Ultrasensitive cascaded in-line Fabry-Perot refractometers based on a C-shaped fiber and the Vernier effect. *Opt. Express* **2022**, *30*, 27704. [[CrossRef](#)] [[PubMed](#)]
22. Singh, A.; Engles, D.; Sharma, A.; Singh, M. Temperature sensitivity of long period fiber grating in SMF-28 fiber. *Optik* **2014**, *125*, 457. [[CrossRef](#)]
23. Kelly, A.; Stearn, R.; McCartney, L. Composite materials of controlled thermal expansion. *Compos. Sci. Technol.* **2006**, *66*, 154. [[CrossRef](#)]
24. Antunes, P.; Domingues, F.; Granada, M.; André, P. *Mechanical Properties of Optical Fibers*; INTECH Open Access Publisher: London, UK, 2012.
25. Norland Optical Adhesive 73. Available online: <https://www.norlandprod.com/adhesives/noa%2073.html> (accessed on 7 December 2023).
26. Song, J.; Sun, S.; Jiang, C.; Chen, N.; Jiang, W.; Liu, C.; Ren, J.; Wang, S. Ultra-sensitive temperature and pressure sensor based on PDMS-based FPI and Vernier effect. *Opt. Lett.* **2023**, *48*, 1674. [[CrossRef](#)] [[PubMed](#)]
27. Huang, B.; Sheng, X.; Tang, Z.; Wang, X.; Lou, S. High and online tunable sensitivity fiber temperature sensor based on Vernier-effect. *Opt. Fiber Technol.* **2022**, *72*, 103003. [[CrossRef](#)]
28. Xu, D.; Gao, H.; Hou, Z.; Zhang, Y.; Tong, X.; Zhang, Y.; Zhang, P.; Shen, J.; Li, C. A High-Sensitivity Fiber-Optic Fabry-Perot Gas Pressure Sensor With Epoxy Resin Adhesive. *IEEE Sens. J.* **2022**, *22*, 10551. [[CrossRef](#)]
29. Mu, X.; Gao, J.; Yang, Y.; Wang, J.; Bi, L. Parallel Polydimethylsiloxane-Cavity Fabry-Perot Interferometric Temperature Sensor Based on Enhanced Vernier Effect. *IEEE Sens. J.* **2022**, *22*, 1333. [[CrossRef](#)]
30. Yang, Y.; Wang, Y.; Zhao, Y.; Jiang, J. Ultrasensitive Temperature Sensor Based on Fiber-Optic Fabry-Perot Interferometer with Vernier Effect. *J. Russ. Laser Res.* **2019**, *40*, 243. [[CrossRef](#)]
31. Wang, F.; Liu, Y.; Lu, Y.; Zhang, L.; Ma, J.; Wang, L.; Sun, W. High-sensitivity Fabry-Perot interferometer temperature sensor probe based on liquid crystal and the Vernier effect. *Opt. Lett.* **2018**, *43*, 5355. [[CrossRef](#)]
32. Hou, L.; Xu, B.; Kang, J.; Zhao, C.; Jin, S. Sensitivity-enhanced Fabry-Perot filled with PDMS temperature sensor based on Vernier effect. In Proceedings of the Asia Communications and Photonics Conference, Hangzhou, China, 26–29 October 2018.
33. Hou, L.; Zhao, C.; Xu, B.; Mao, B.; Shen, C.; Wang, D.N. Highly sensitive PDMS-filled Fabry-Perot interferometer temperature sensor based on the Vernier effect. *Appl. Opt.* **2019**, *58*, 4858. [[CrossRef](#)]

34. Liang, J.; Qu, J.; Ye, J.; Liu, Y.; Qu, S. Ultra-Sensitive Temperature Sensor of Cascaded Dual PDMS-Cavity Based on Enhanced Vernier Effect. *IEEE Sens. J.* **2023**, *23*, 2264. [[CrossRef](#)]
35. Pan, R.; Liu, M.; Bian, Y.; Xu, T.; Yang, W.; Yang, Y.; Wang, J.; Mu, X.; Bi, L. High-sensitive temperature sensor with parallel PDMS-filled FPIs based on dual Vernier effect. *Opt. Commun.* **2022**, *518*, 128284. [[CrossRef](#)]

Disclaimer/Publisher's Note: The statements, opinions and data contained in all publications are solely those of the individual author(s) and contributor(s) and not of MDPI and/or the editor(s). MDPI and/or the editor(s) disclaim responsibility for any injury to people or property resulting from any ideas, methods, instructions or products referred to in the content.